The Journal of Chemical Physics ARTICLE scitation.org/journal/jcp

Stereoinversion of tetrahedral *p*-block element hydrides

Cite as: J. Chem. Phys. 156, 194113 (2022); doi: 10.1063/5.0090267
Submitted: 4 March 2022 • Accepted: 2 May 2022 •
Published Online: 20 May 2022

Lukas M. Sigmund,[1] Christopher Ehlert,[2] Ganna Gryn'ova,[2] and Lutz Greb[3,a)]

AFFILIATIONS

[1] Anorganisch-Chemisches Institut, Ruprecht-Karls-Universität Heidelberg, Im Neuenheimer Feld 270, 69120 Heidelberg, Germany

[2] Heidelberg Institute for Theoretical Studies (HITS gGmbH), Schloss-Wolfsbrunnenweg 35, 69118 Heidelberg, Germany and Interdisciplinary Center for Scientific Computing (IWR), Ruprecht-Karls-Universität Heidelberg, Im Neuenheimer Feld 205, 69120 Heidelberg, Germany

[3] Anorganische Chemie, Freie Universität Berlin, Fabeckstraße 34-36, 14195 Berlin, Germany

Note: This paper is part of the JCP Special Topic on Nature of the Chemical Bond.
[a)] **Author to whom correspondence should be addressed:** lutz.greb@fu-berlin.de

ABSTRACT

The potential energy surfaces of 15 tetrahedral *p*-block element hydrides were screened on the multireference level. It was addressed whether stereoinversion competes against other reactions, such as reductive H_2-elimination or hydride loss, and if so, along which pathway the stereomutation occurs. Importantly, stereoinversion transition structures for the ammonium cation (C_{4v}) and the tetrahydridoborate anion (C_s) were identified for the first time. Revisiting methane's C_s symmetric inversion transition structure with the mHEAT+ protocol revealed an activation enthalpy for stereoinversion, in contrast to all earlier studies, which is 5 kJ mol^{-1} *below* the C–H bond dissociation enthalpy. Square planar structures were identified lowest in energy only for the inversion of AlH_4^-, but a novel stepwise C_s-inversion was discovered for SiH_4 or PH_4^+. Overall, the present contribution delineates essentials of the potential energy surfaces of *p*-block element hydrides, while structure–energy relations offer design principles for the synthetically emerging field of structurally constrained compounds.

INTRODUCTION

The configurational stability of tetrasubstituted carbon is at the heart of (bio)organic chemistry; e.g., it allows for the construction of enzymes with structure–activity relationships relying on the *homochiral* feedstock of the naturally occurring amino acids. The archetypical tetrasubstituted carbon compound, methane, was intensively studied concerning its stereochemical inversion.[1–9] Eventually, it was shown by Gordon and Schmidt[10] and by Pepper *et al.*[11] that stereoinversion might occur not through a square planar—as speculated before—but rather via a C_s symmetric transition state [Fig. 1(a)]. Notably, the planarization of CH_4 is energetically significantly more demanding than the distortion to the C_s symmetric transition state. In addition, the D_{4h} state is a higher-order saddle point on the potential energy surface (PES), ruling out inversion of methane via a square planar transition structure. However, a tenet since then was that methane's inversion through the C_s symmetric transition state is prohibited by the more favorable C–H bond dissociation enthalpy (439.3 ± 0.4 kJ mol^{-1})[12,13] by ~20 to 30 kJ mol^{-1}.[10,11]

The situation changes by replacing carbon with other *p*-block elements or by altering the substituents. Proper square planar inversion transition states were identified for SiH_4 and GeH_4 [Fig. 1(b)].[6,14] Higher substituted group 14-based compounds were also investigated for square planar inversion,[15–17] and significant attention was paid to approaches for the stabilization of square planar configurations as ground state (GS) geometries.[18–34] In parallel to the theoretical efforts, remarkable progress was made in the experimental realization of square planar-coordinated *p*-block elements.[35–45]

However, the structural flexibility of tetrahedral compounds is far from being exhaustively understood, and groups 13 and 15 of the Periodic Table are notably less investigated.[46–49] Recently, our group reported >250 planar inversion transition states for

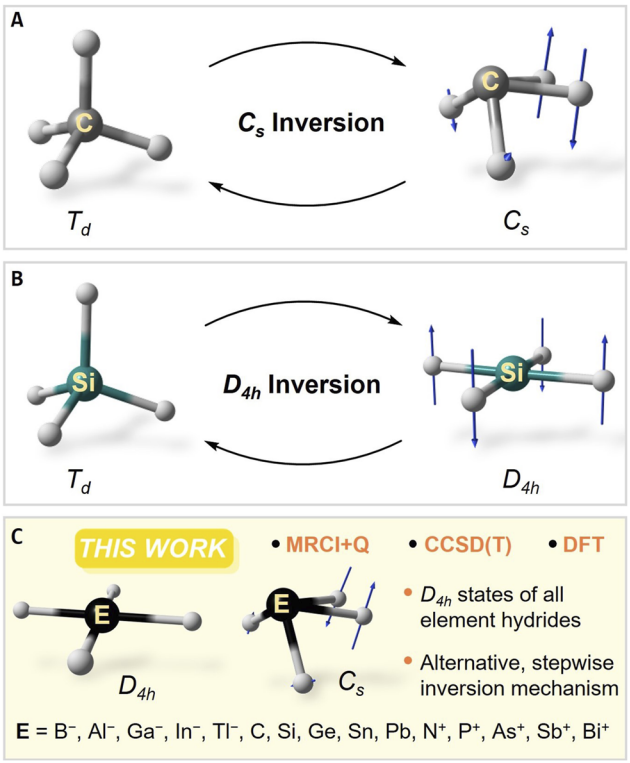

FIG. 1. Inversion mechanism of (a) methane, via a C_s symmetric transition state, and (b) of silane, via a square planar D_{4h} symmetric transition structure. (c) D_{4h} symmetric states and a lower-symmetric inversion mechanism of 15 *p*-block element hydrides covered in this work. The scaled displacement vectors of imaginary modes are shown in blue.

group 13-, 14-, and 15-based compounds.[50] It was shown that the introduction of non-hydrogen substituents drastically lowers the inversion activation barrier to values superable at mild temperatures. Moreover, a qualitative mnemonic for assessing the inversion barrier height was developed by its analysis according to the second-order Jahn–Teller effect.[51–54] Large energetic separations of the highest occupied (HOMO) and lowest unoccupied molecular orbital (LUMO) in the inversion transition state result in low activation barriers and vice versa.

The energetic penalty for transforming from the tetrahedral to the square planar state can be understood qualitatively from Walsh-type diagrams of a given *p*-block element hydride [Fig. 2(a)].[55] The two t_2 molecular orbital (MO) representations of the tetrahedral ground state decompose to two e_u sets as well as to a_{2u} and b_{1g} representations, respectively. The highest occupied MO turns from bonding to non-bonding, experiencing a significant increase in energy, which causes the substantial activation barrier for inversion. The energetic separation of the highest occupied and lowest unoccupied MO (HOMO–LUMO gap) in the square planar state, the a_{2u} and b_{1g} MO, substantially decreases compared to the tetrahedral ground state. This close orbital approach allows several electronic configurations [Figs. 2(b)–2(e)]: the closed-shell singlet δ- configuration [doubly occupied b_{1g} MO, 1 $^1A_{1g}$, Fig. 2(b)] and π-configuration [doubly occupied a_{2u} MO, 2 $^1A_{1g}$, Fig. 2(c)], the open-shell singlet configuration, and the corresponding triplet configuration [both singly occupied a_{2u} and b_{1g} MO, $^1B_{2u}$, and $^3B_{2u}$, respectively; Fig. 2(d) or Fig. 2(e)].

Accordingly, not only a wealth of electronic configurations needs to be considered for the stereoinversion of *p*-block element tetrahedrons, but also pathways along other structural arrangements are possible. Consequently, multireference computations and an ample structural space are required to allow ultimate statements on the "true" stereoinversion pathways and other fates of tetrahedral group 13, 14, and 15 element hydrides.

This is the purpose of the present work, which is divided into two parts [Fig. 1(c)]. The section titled Computational Methods discusses the square planar states of the element hydrides of the second through the sixth period of the Periodic Table based on *ab initio* calculations on the complete active space self-consistent field method (CASSCF) and multireference configuration interaction (MRCI)+Q level. The lowest-energy electronic configurations are identified and evaluated concerning their harmonic vibrations and their relevance as inversion transition states. In the section titled Results and Discussion, non-planar structures of all element hydrides

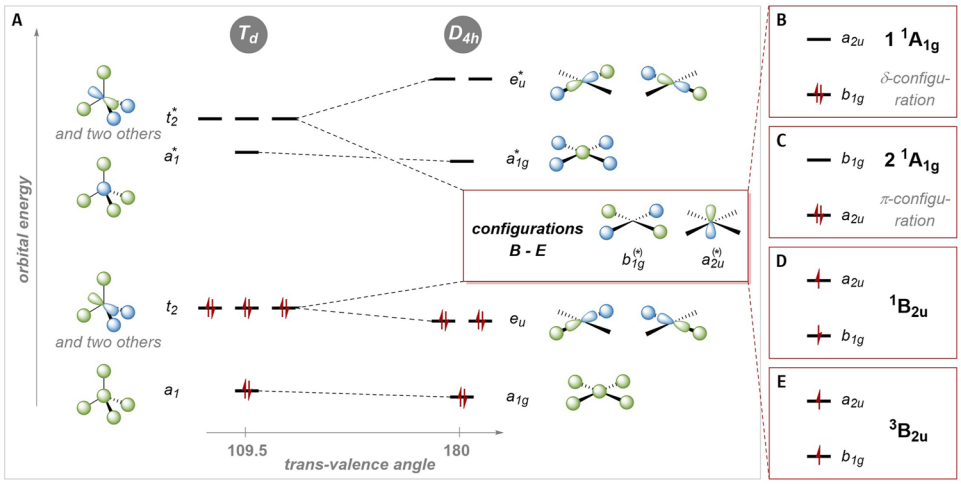

FIG. 2. (a) Schematic Walsh diagram for the transformation of a *p*-block element hydride from the tetrahedral to the square planar state and (b)–(e) the potential electronic configurations of the square planar state.

and their potential role in alternative inversion mechanisms are inspected—including the reevaluation of methane's stereoinversion. All possible inversion mechanisms are weighed against each other and competing reactions, e.g., E–H bond dissociation or the elimination of molecular hydrogen.

COMPUTATIONAL METHODS

To cover all potentially relevant electronic configurations [see Figs. 2(b)–2(e)] of the square planar structures of D_{4h} symmetry, a state-specific multiconfigurational level was applied. Structure

TABLE I. Lowest energies/enthalpies of the singlet and triplet states of the square planar (D_{4h}) configurations of EH_4^n. In case only one number is given, the electronic energy is meant. The number of imaginary harmonic vibrations and their symmetry are given. All numbers were obtained on the MRCI+Q/aug-cc-pwCVQZ(-PP)//CASSCF(8e,8o)/aug-cc-pwCVQZ(-PP) computational level. For the data of the higher energy electronic configurations, see Table S1 in the supplementary material.

		BH_4^-	AlH_4^-	GaH_4^-	InH_4^-	TlH_4^-
Singlet	E/H (kJ mol^{-1})	477.3	222.3/215.4	279.7/268.0	235.0/225.5	246.8/233.7
	El. config.	$^1B_{2u}$	$1\,^1A_{1g}$ (δ)	$1\,^1A_{1g}$ (δ)	$1\,^1A_{1g}$ (δ)	$1\,^1A_{1g}$ (δ)
	Imag. vib.	3; B_{2u}, E_u	1; B_{2u}	1; B_{2u}	1; B_{2u}	1; B_{2u}
Triplet	E (kJ mol^{-1})	475.5	421.1	404.1	365.8	330.4
	Imag. vib.	2; E_u	3; E_u, A_{2u}	3; E_u, A_{2u}	3; A_{2u}, E_u	4; A_{2u}, E_u, B_{1g}
		CH_4	SiH_4	GeH_4	SnH_4	PbH_4
Singlet	E/H (kJ mol^{-1})	571.4	376.6/369.5	419.1/407.3	333.5/323.9	326.6/313.6
	El. config.	$2\,^1A_{1g}$ (π)	$1\,^1A_{1g}$ (δ)	$1\,^1A_{1g}$ (δ)	$1\,^1A_{1g}$ (δ)	$1\,^1A_{1g}$ (δ)
	Imag. vib.	4; B_{2u}, A_{2u}, E_u	1; B_{2u}	1; B_{2u}	1; B_{2u}	1; B_{2u}
Triplet	E (kJ mol^{-1})	680.0	482.2	468.5	416.7	387.5
	Imag. vib.	1; B_{1g}	3; A_{2u}, E_u	3; A_{2u}, E_u	3; A_{2u}, E_u	3; A_{2u}, E_u
		NH_4^+	PH_4^+	AsH_4^+	SbH_4^+	BiH_4^+
Singlet	E/H (kJ mol^{-1})	485.4	518.5/481.0	493.5	426.0	401.4
	El. config.	$2\,^1A_{1g}$ (π)	$^1B_{2u}$	$^1B_{2u}$	$^1B_{2u}$	$^1B_{2u}$
	Imag. vib.	4; B_{2u}, A_{2u}, E_u	1; B_{2u}	3; B_{2u}, E_u	4; B_{2u}, E_u, A_{2u}	4; B_{2u}, E_u, A_{2u}
Triplet	E (kJ mol^{-1})	923.0	519.7	501.1	435.9	409.5
	Imag. vib.	3; B_{1g}, E_u	3; A_{2u}, E_u	3; A_{2u}, E_u	3; A_{2u}, E_u	3; A_{2u}, E_u

TABLE II. Inversion transition structures with scaled displacement vectors of the single imaginary vibrational mode of BH_4^-, CH_4, and NH_4^+; their energy/enthalpy relative to the tetrahedral ground states; and selected structural characteristics. Energies in kJ mol^{-1} were obtained on the CCSD(T)/aug-cc-pwCVQZ//CCSD(T)/aug-cc-pwCVTZ computational level. "Lowest energy competition reaction" means the lowest-energy reaction among those given in Scheme 1, and "D_{4h} minimum" means the lowest energy of a square planar structure along with its electronic configuration [see Figs. 2(b)–2(e)].

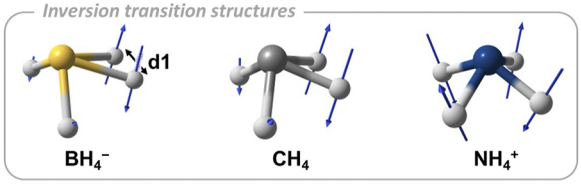

	BH_4^-	CH_4	NH_4^+
Inversion barrier ($\Delta E^‡/\Delta H^‡$)	368.3/361.1	457.9/436.0	439.1/404.8
Lowest energy competition reaction ($\Delta E/\Delta H$)	320.0/307.1 (loss of H^-)	469.4/436.4 (loss of $H^·$)	558.1/519.9 (loss of $H^·$)
D_{4h} minimum ($\Delta E^‡$)	475.5 ($^3B_{2u}$)	571.4 ($2\,^1A_{1g}$)	485.4 ($2\,^1A_{1g}$)
Molecular point group	C_s	C_s	C_{4v}
Ground state bond length (pm)	123.6	108.8	102.2
Transition state bond lengths (pm)	122.8/145.3	111.3/121.1	106.9
d1 (pm)	80.4	91.6	134.9
trans-valence angle (deg)	105.4	110.1	126.4

optimizations and numerical harmonic frequency calculations were carried out with the complete active space self-consistent field method (CASSCF).[56] The active space included the full valence space, resulting in a CAS(8*e*,8*o*). The aug-cc-pwCVQZ set of basis functions was used for B, C, N, Al, Si, and P atoms. Hydrogen atoms were described with the aug-cc-pVQZ basis set. For the heavier elements, such as Ga, Ge, As, In, Sn, Sb, Tl, Pb, and Bi, Stuttgart–Köln MCDHF RSC effective core potentials (ECPs) were applied with the respective ECP-based aug-cc-pwCVQZ-PP basis set. No frozen core approximation was used. Final single point electronic energies were obtained from multireference configuration interaction calculations, including the Davidson correction for

TABLE III. Stationary points of the stepwise inversion mechanism and dissociative competition pathway with the scaled displacement vectors of the single imaginary mode of the transition states of $\mathbf{EH_4^n}$ (**E** = Al^-, Ga^-, In^-, Tl^-, Si, Ge, Sn, Pb, P^+, As^+, Sb^+, and Bi^+). All given energies/enthalpies are relative to the respective tetrahedral ground states (**GS**). Entry 4 gives the barrier heights for the oxidative addition of the H_2 fragment, entry 5 gives the dissociation energy/enthalpy of the **Int** structures into H_2 and the $\mathbf{EH_2^n}$ fragment, and entry 6 gives the energy/enthalpy of the lowest D_{4h} symmetric structures. If not mentioned otherwise, all numbers were obtained on the CCSD(T)/aug-cc-pwCVQZ(-PP)//CCSD(T)/aug-cc-pwCVTZ(-PP) computational level and are given in kJ mol^{-1}.

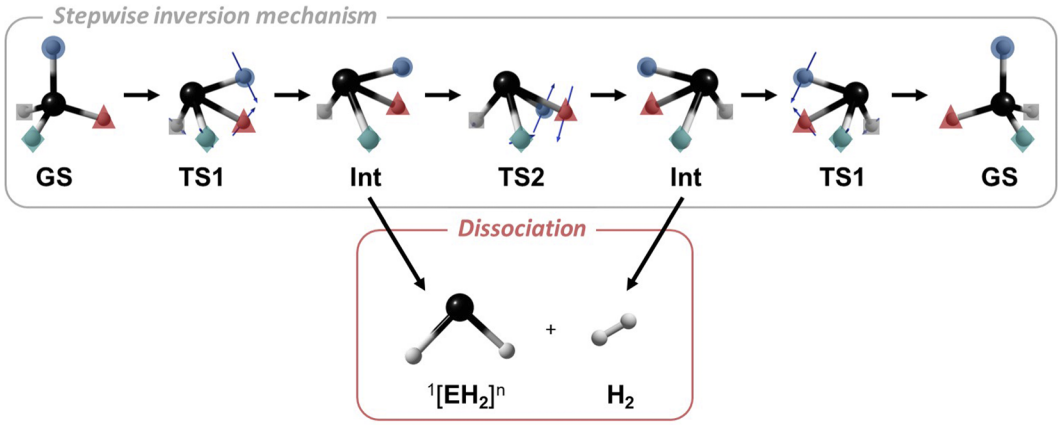

Entry	State	AlH_4^-	GaH_4^-	InH_4^-	TlH_4^-
1	**TS1** ($\Delta E^‡/\Delta H^‡$)	234.7/227.4	211.7/203.1	200.9/193.2	168.3/159.9
2	**Int** ($\Delta E/\Delta H$)	196.4/196.8	152.2/149.4	91.6/89.8[a]	11.8/9.1[a]
3	**TS2** ($\Delta E^‡/\Delta H^‡$)	200.7/196.5	*Not found*	93.4/91.3	13.2/10.4
4	**Int** ⟶ **TS1** ($\Delta E^‡/\Delta H^‡$)	38.3/30.6	59.5/53.7	109.3/103.4	156.5/150.8
5	**Int** ⟶ H_2 + $^1[\mathbf{EH_2^n}]$ ($\Delta E/\Delta H$)	10.1/3.2	10.2/4.3	7.6/5.2	7.6/5.4
6	D_{4h} minimum ($\Delta E^‡/\Delta H^‡$)	222.4/215.3 ($1\,^1A_{1g}$)	280.5/268.2 ($1\,^1A_{1g}$)	235.9/225.5 ($1\,^1A_{1g}$)	248.7/234.4 ($1\,^1A_{1g}$)

Entry	State	SiH_4	GeH_4	SnH_4	PbH_4
1	**TS1** ($\Delta E^‡/\Delta H^‡$)	248.1/235.8	218.6/206.3	207.2/196.8	167.6/157.1
2	**Int** ($\Delta E/\Delta H$)	222.7/217.4	155.0/148.7	81.8/79.2	−22.4/−24.0
3	**TS2** ($\Delta E^‡/\Delta H^‡$)	236.0/226.2	160.6/150.5	84.1/78.5	−21.2/−25.5
4	**Int** ⟶ **TS1** ($\Delta E^‡/\Delta H^‡$)	25.4/18.4	63.6/57.6	125.4/117.6	190.0/181.1
5	**Int** ⟶ H_2 + $^1[\mathbf{EH_2^n}]$ ($\Delta E/\Delta H$)	33.6/21.6	22.7/13.3	14.9/8.0	13.1/7.1
6	D_{4h} minimum ($\Delta E^‡/\Delta H^‡$)	378.6/371.0 ($1\,^1A_{1g}$)	421.3/408.6 ($1\,^1A_{1g}$)	335.7/325.2 ($1\,^1A_{1g}$)	329.5/315.2 ($1\,^1A_{1g}$)

Entry	State	PH_4^+	AsH_4^+	SbH_4^+	BiH_4^+
1	**TS1** ($\Delta E^‡/\Delta H^‡$)	226.1/210.7	196.2/181.7	189.4/177.1	146.7/133.9
2	**Int** ($\Delta E/\Delta H$)	217.5/208.9	145.1/138.7	68.3/65.8	−42.6/−43.3
3	**TS2** ($\Delta E^‡/\Delta H^‡$)	239.2/227.9	154.7/145.0	72.4/66.9	−40.7/−44.1
4	**Int** ⟶ **TS1** ($\Delta E^‡/\Delta H^‡$)	8.6/1.8	51.1/43.0	121.1/111.3	189.3/177.2
5	**Int** ⟶ H_2 + $^1[\mathbf{EH_2^n}]$ ($\Delta E/\Delta H$)	133.5/119.2	94.3/82.0	59.1/49.8	47.8/39.9
6	D_{4h} minimum (ΔE)	518.5[b] ($^1B_{2u}$)	493.5[b] ($^1B_{2u}$)	426.0[b] ($^1B_{2u}$)	401.4[b] ($^1B_{2u}$)

[a]Structure has a single imaginary frequency.
[b]Calculated at the MRCI+Q/aug-cc-pwCVQZ(-PP)//CASSCF(8*e*,8*o*)/aug-cc-pwCVQZ(-PP) level of theory.

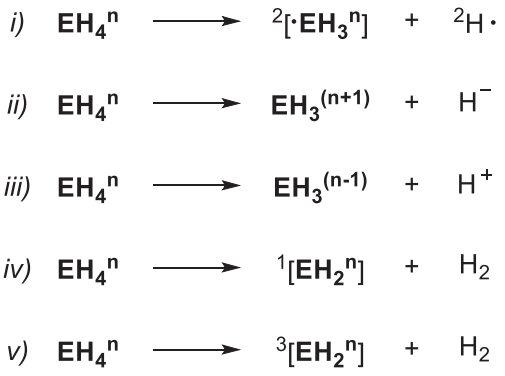

SCHEME 1. Reactions that compete with the stereoinversion processes.

unlinked quadruples (MRCI+Q).[57,58] The CASSCF wave functions were used as multiconfigurational reference. The same basis set and ECP strategy as for the CASSCF calculations were deployed. All MCSCF and MRCI+Q calculations were done with the MOLPRO 2020.1 quantum chemistry package.[59,60] For some D_{4h} structures, the numerical frequency calculations with the CASSCF method proved problematic and were eventually prohibited due to root-flipping, which occurred for specific displaced structures (see the supplementary material for further details). Fortunately, this problem did not occur for the lowest-energy cases, which are reported below (Table I).

Coupled cluster calculations, including singles and doubles with perturbative triples corrections [CCSD(T)],[61–63] were used to investigate the lower symmetric inversion mechanisms (cf. Tables II and III), the competing side reactions (Scheme 1), and other structures on the respective PESs. The same basis set, ECP, and frozen core settings as for the MRCI+Q calculations were employed, except for the application of the respective triple-ζ basis sets [aug-cc-pwCVTZ(-PP)] for structure optimizations and the computations of harmonic frequencies. Where possible, the obtained numbers were compared to experimentally determined values (see Chap. S7 in the supplementary material). Good to excellent agreement was found (MAD of 4.4 kJ mol^{-1}). For the CCSD(T) calculations, ORCA 4.2.1 was used.[64,65]

Transition structures were verified by their single imaginary mode of desired symmetry and by applying intrinsic reaction coordinate (IRC) calculations in both directions. If not mentioned otherwise, relative energies are given as enthalpies at 298.15 K and in kJ mol^{-1}. The respective thermal corrections were obtained from the harmonic vibrational analyses and were combined with the electronic energies of the final single-point calculations. Frontier molecular orbital energies are discussed based on Kohn–Sham density functional theory (KS-DFT) calculations with the B97M-D3(BJ) functional and the def2-QZVPP basis set using the CCSD(T) structures. For any further computational details, see the supplementary material.

RESULTS AND DISCUSSION

Evaluation of D_{4h} symmetric structures

The structures of the square planar element hydrides were optimized under a D_{4h} symmetry constraint in the four considered electronic configurations [see Figs. 2(b)–2(e)]. Table I lists the lowest-energy singlet and triplet state configurations (data for all other states can be found in the supplementary material). The results are discussed based on electronic energies, as some structures represent higher-order saddle points on the respective PESs.

The D_{4h} symmetric structures correspond to transition states (one imaginary frequency of B_{2u} symmetry, $\mathbf{TS_{D4h}}$) for $\mathbf{EH_4^n}$ with $\mathbf{E^n}$ = Al$^-$, Ga$^-$, In$^-$, Tl$^-$, Si, Ge, Sn, Pb, and P$^+$. Importantly, for all $\mathbf{EH_4^n}$, except AlH$_4^-$, these square planar structures do not correspond to the lowest energy transition states, as will be discussed further below. For $\mathbf{EH_4^n}$ with $\mathbf{E^n}$ = B$^-$, C, N$^+$, As$^+$, Sb$^+$, and Bi$^+$, the D_{4h} symmetric structures are higher-order saddle points with more than one imaginary frequency.

For D_{4h} symmetric BH$_4^-$, the triplet state (476 kJ mol^{-1}) is more favorable but only slightly below the open-shell singlet configuration (477 kJ mol^{-1}). The latter possesses three imaginary vibrations, the prior two. Owing to the enormous energetic demands to achieve square planar BH$_4^-$ and the absence of a single imaginary mode of B_{2u} symmetry for both electronic configurations, the structural inversion of the tetrahydridoborate anion through a square planar state can be ruled out. For methane, we qualitatively reproduced the results of Gordon and Schmidt,[10] that is, the preference for the closed-shell singlet 2 ^{1}A$_{1g}$ configuration in square planar CH$_4$ with four imaginary vibrational modes. However, with the more elaborated MRCI+Q/aug-cc-pwCVQZ computational procedure, significantly lower planarization energies were obtained compared to those of Gordon and Schmidt [e.g., 571 vs 663 kJ mol^{-1} at the SOCI/6-31G(d,p) computational level for the 2 ^{1}A$_{1g}$ state]. For the ammonium cation, we can also conclude that the square planar inversion is not possible. The lowest-energy singlet state (485 kJ mol^{-1}) represents, as in the case of CH$_4$, a higher-order saddle point. The same holds for the triplet state, which is additionally associated with an exorbitant increase in electronic energy (923 kJ mol^{-1}).

Thus, distortion of the second-period element hydrides to D_{4h} symmetry comes with enormous energy demands and does not provide a feasible pathway for stereochemical inversion. This situation significantly changes when the D_{4h} symmetric structures for the heavier homologs of groups 13 and 14 are inspected ($\mathbf{EH_4^n}$ with $\mathbf{E^n}$ = Al$^-$, Ga$^-$, In$^-$, Tl$^-$, Si, Ge, Sn, and Pb). They are all characterized by a lowest-energy 1 ^{1}A$_{1g}$ electronic configuration, with all the other configurations being significantly higher in energy. Moreover, they all feature a single imaginary mode of B_{2u} symmetry. Therefore, the square planar structures represent inversion transition states ($\mathbf{TS_{D4h}}$), as indicated for some of the considered molecules before.[6,16,50] Group 14 element hydrides invert at higher enthalpies as group 13-based compounds do. Within a given group, they find maxima for the fourth-period cases (GaH$_4^-$, GeH$_4$).

For the square planar states of the heavier element hydrides of group 15 ($\mathbf{EH_4^n}$ with $\mathbf{E^n}$ = P$^+$, As$^+$, Sb$^+$, and Bi$^+$), the open-shell singlet configurations were found lowest in energy, slightly below the triplet states. The associated planarization energies are very high, exceeding those of group 13 and 14 compounds. The frequency analyses revealed a single imaginary mode of B_{2u} symmetry for PH$_4^+$ and, thus, a proper inversion transition state (481 kJ mol^{-1} activation enthalpy). In the orbital picture, the preferred open-shell nature of D_{4h} symmetric group 15 hydrides might be explained by the close approach of HOMO and LUMO [Fig. 2(a)], as well as by the orbital-contracted nature due to the positive charge.

Evaluation of lower symmetry inversion processes and a comparison with competing pathways

The evaluation of the D_{4h} symmetric structures on the multi-configurational level identified inversion transition states for nine of the 15 considered element hydrides. To probe if the processes via the square planar transition structure ("D_{4h}-*inversion*") indeed corresponds to the lowest-energy possibility and to identify the energetically most favorable pathways of stereoinversion for the remaining species, structures of lower symmetry were considered. Moreover, to allow a statement on the general feasibility of stereoinversion, reaction and activation enthalpies of dissociative processes were also evaluated (Scheme 1).[46] These are (*i*) homolytic E–H bond dissociation, heterolytic bond scission; the loss of (*ii*) a hydride or (*iii*) a proton, or the elimination of molecular hydrogen to afford $\mathbf{EH_2}^{\mathbf{n}}$ species, either of (*iv*) singlet or (*v*) triplet electronic configuration.

These pathways were investigated for the considered compounds. The critical results are discussed in the following. A summary of all data is given in the supplementary material in Chap. S6. Optimizations of minimum and transition structures and frequency analyses were carried out with the CCSD(T)/aug-cc-pwCVTZ(-PP) method. All final energies were obtained at the higher CCSD(T)/aug-cc-pwCVQZ(-PP) level of theory.

A transition state of C_s symmetry was obtained for the BH_4^- anion (Table II). It features two markedly different pairs of hydrogen atoms and can thus be interpreted as a complex of the dihydroboryl anion with side-on coordinating H_2. Frequency analysis and IRC calculation confirmed that the structure corresponds to an inversion transition state with $\Delta H^{\ddagger}$ = 361 kJ mol^{-1}. However, the low gas-phase hydride affinity of BH_3 (calculated to 307 kJ mol^{-1}, experimental value: 310 ± 12 kJ mol^{-1})[66,67] rules out stereoinversion of BH_4^- instead of hydride expulsion. Consequently, a non-dissociative stereoinversion of BH_4^- in the gas phase is unlikely.

For the NH_4^+ cation, the transition state search converged to a square pyramidal structure (C_{4v} symmetry, Table II). Calculation of the harmonic frequencies and IRC computations validated the inversion transition structure. It comes with a high activation enthalpy of 405 kJ mol^{-1}. Nevertheless, it is considerably lower in energy than *all* potentially competing processes (Scheme 1, homolytic bond cleavage has the lowest reaction enthalpy of 520 kJ mol^{-1}). Hence, the intramolecular stereoinversion of the ammonium cation is enthalpically feasible. Of note, the C_{4v} symmetry of the inversion transition state of the ammonium cation was briefly noted by Pepper *et al.* in their seminal work on CH_4 but got never further elaborated.[11]

We also recalculated the inversion barrier of methane via the C_s symmetric transition state (Table II). Gordon and Schmidt as well as Pepper *et al.* concluded from their results that the stereoinversion of methane is not possible because of the homolytic bond dissociation enthalpy, which was experimentally determined to 439.3 ± 0.4 kJ mol^{-1}.[12,13] With the CCSD(T)/aug-cc-pwCVQZ//CCSD(T)/aug-cc-pwCVTZ computational method, we obtained an inversion activation enthalpy of 436 kJ mol^{-1}. As this value is still within the error range of the CH-bond dissociation (given the applied computational method), an even more precise barrier height for the stereochemical inversion of CH_4 was determined with the modified high-accuracy extrapolated *ab initio* thermochemistry protocol (mHEAT+).[68–71] The CFOUR quantum chemistry software package was used for this purpose.[72] An activation enthalpy of 434.2 kJ mol^{-1} was obtained, which is 5.1 kJ mol^{-1} (1.22 kcal mol^{-1}) below the experimentally obtained C–H bond dissociation enthalpy. Considering these results, the intramolecular stereoinversion of methane via the C_s symmetric transition state appears enthalpically feasible and not prohibited by the strength of the C–H bond (Fig. 3).

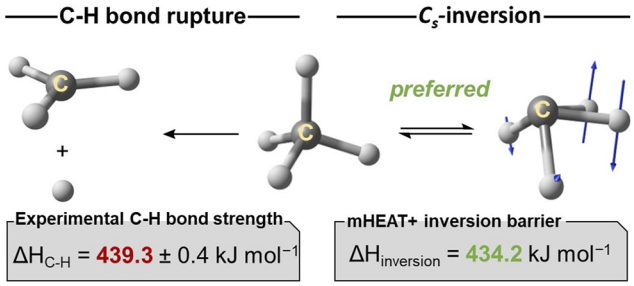

FIG. 3. Comparison of the experimentally determined bond dissociation enthalpy [reaction (*i*) in Scheme 1] vs the C_s-*inversion* and the associated activation enthalpy calculated with the mHEAT+ protocol for methane.

Next, C_s symmetric structures were probed for the heavier homologs. Except for GaH_4^-, C_s symmetric transition structures (**TS2**, Table III) were located for all heavier *p*-block element hydrides. The IRCs were followed in both directions along the single A'' symmetric imaginary modes. Without exception, the IRCs did not converge to the tetrahedral ground states but instead to a new structure (**Int**, Table III), also of C_s symmetry.[73] These minimum structures can be viewed as σ-complexes of molecular hydrogen coordinating to the two-electron-reduced $\mathbf{EH_2}^{\mathbf{n}}$ fragments.

Indeed, such **Int** structures of group 14 element compounds were debated as post-complexes in the context of reductive elimination of H_2 from the tetrahedral $\mathbf{EH_4}$ or as pre-complexes during the oxidative addition of dihydrogen to $\mathbf{EH_2}$.[74–85] Of note, Merino *et al.* compared their calculated scaled harmonic vibrations (B3LYP/LANL2DZ+dp) of the **Int** structure of SiH_4 and GeH_4 with previously unassigned bands in IR spectra experimentally obtained from matrix isolation experiments and found remarkable agreement.[79] Our calculations now suggest such intermediates, also for isoelectronic group 13 and group 15 compounds, and for the first time as possible intermediates during stereoinversion. To reach the **Int** structures from the tetrahedral ground states, the reductive elimination transition states **TS1** need to be surpassed. They were computed for all compounds (Table III).

When the three stationary points (**TS1**, **Int**, and **TS2**) are combined, a new mechanism for the stereoinversion of tetrasubstituted *p*-block elements arises, which is denoted *stepwise* C_s-*inversion*. Starting from the tetrahedral ground state, it consists of the rate-determining reductive semi-elimination of H_2 (**TS1**) to give **Int** in which H_2 remains bound within a σ-complex. The rotation of the H_2 fragment via **TS2** proceeds with a minimal activation barrier, and a final oxidative-addition-type step (**TS1**) furnishes the inverted molecule. The barrier height for the rate-determining semi-elimination decreases within a given group of the Periodic Table when going from top to bottom (cf. Table III, entry 1). According to the Bell–Evans–Polanyi principle,[86–88] this is consistent with the increasing stability of lower oxidation states for the heavier elements.

The lowest activation enthalpies were found for group 15 compounds (211–134 kJ mol^{-1}), followed by group 13 species (227–160 kJ mol^{-1}) and group 14-based molecules (236–157 kJ mol^{-1}). Our numbers are in good agreement with the CCSD(T) values of Merino *et al.* obtained for group 14 element hydrides.[79]

Strikingly, comparing the energies with the D_{4h}-*inversion* (Table III, entry 6), this reductive semi-elimination/H_2-rotation/oxidative addition process (*stepwise* C_s-*inversion*) becomes the favored pathway for stereoinversion for most of the element hydrides. The activation enthalpies for the D_{4h}-*inversion*, either of 1 $^1A_{1g}$ (**EH$_4$**, **E** = Al$^-$, Ga$^-$, In$^-$, Tl$^-$, Si, Ge, Sn, Pb) or $^1B_{2u}$ (**EH$_4$**, **E** = P$^+$) electronic configuration, are substantially higher as the barriers of the *stepwise* C_s-*inversion* (e.g., for PH_4^+, the enthalpy difference is 270 kJ mol^{-1}, and for SiH_4, it is 135 kJ mol^{-1}) and increase when going from left to right in the Periodic Table. Correspondingly, only for AlH_4^-, the D_{4h}-*inversion* is favored over the *stepwise* C_s-*inversion* by 12 kJ mol^{-1}. Notably, the D_{4h}-*inversion* is also preferred against all considered competing reactions (see Scheme 1), including the loss of a hydride anion (315 kJ mol^{-1}) or the elimination of H_2 (227 kJ mol^{-1} activation enthalpy). Thus, it can be concluded that AlH_4^- undergoes stereochemical inversion via **TS$_{D4h}$** with an activation enthalpy of 215 kJ mol^{-1}.

To understand the differences between the D_{4h}-*inversion* and the *stepwise* C_s-*inversion* mechanism, the electronic structures of **TS1** and **TS$_{D4h}$** were investigated for AlH_4^- in comparison to SiH_4. This was done by following the respective IRCs and subsequent calculation of molecular orbital energies for the individual IRC pictures on the B97M-D3(BJ)/def2-QZVPP level of theory (Fig. 4). In either case, the transformation toward the transition structure increases the energy of one of the MOs of the triply degenerate fully occupied t_2 representation. For AlH_4^- [Fig. 4(a)], this increase is slightly stronger for the C_s path (2.61 vs 2.15 eV and 252 vs 207 kJ mol^{-1}, respectively) but gets counterbalanced by the stabilization of the three other valence MOs (−4.16 eV, −401 kJ mol^{-1} in total). In **TS$_{D4h}$** of AlH_4^-, this stabilizing effect is less intense (−0.45 eV, −43 kJ mol^{-1}). In total, both paths are energetically almost identical, with the square planar inversion being marginally favored. For SiH_4 [Fig. 4(b)], the C_s symmetric path experiences a diminished increase in the occupied orbital energies compared to the path to D_{4h} symmetry (2.68 vs 3.44 eV and 259 vs 332 kJ mol^{-1}, respectively). At the same time, the stabilization of the other orbitals remains substantial (−2.47 eV, −238 kJ mol^{-1}) and further supports **TS1**. The stabilizing contribution in **TS$_{D4h}$** is only −0.93 eV (−90 kJ mol^{-1}). This picture rationalizes that the semi-elimination of H_2 from SiH_4 is energetically more favorable than the ascent of the square planar inversion transition state by 131 kJ mol^{-1} in electronic energy ($\Delta\Delta H^{\ddagger}$ = 135 kJ mol^{-1}). The same was found for the other investigated element hydrides (see Table S12 in the supplementary material).

Having evaluated the C_s against the D_{4h} pathway, it was considered if the *stepwise* C_s-*inversion* can compete with the alternative reaction channels given in Scheme 1. The enthalpically most favorable competition reaction for the third to sixth-period element hydrides is in all cases the elimination of H_2 from **EH$_4^n$** to give singlet **EH$_2^n$** [reaction (*iv*) in Scheme 1; see Table S6 in the supplementary material]. If the semi-eliminated H_2 in **Int** leaves the coordination sphere of **EH$_2^n$** (H_2 elimination) or rotates via **TS2** and

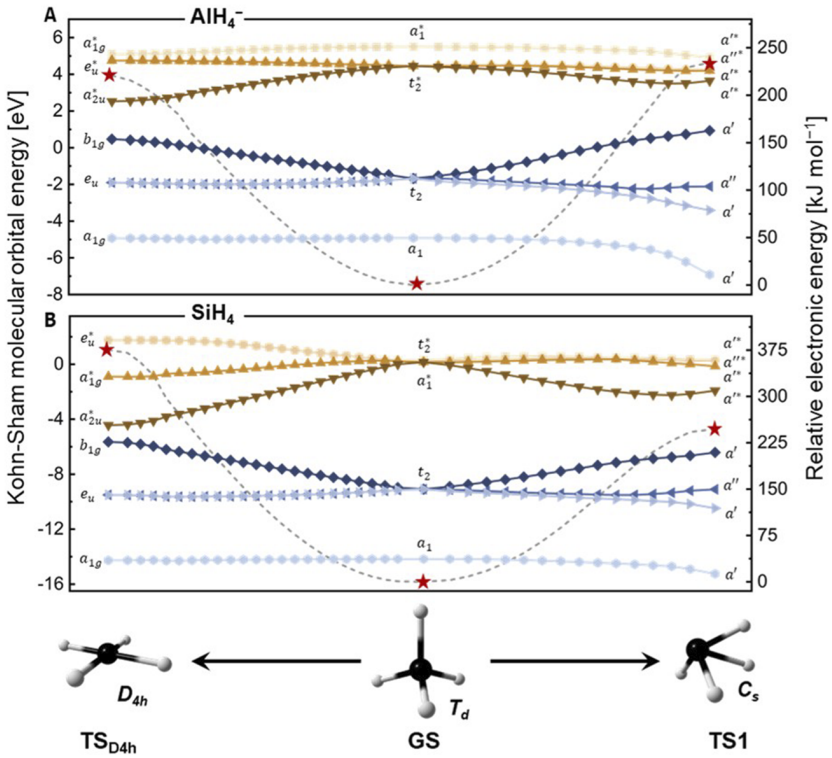

FIG. 4. Kohn–Sham frontier molecular orbital energies of the individual IRC pictures of the transformation of the tetrahedral ground state to the D_{4h} (**TS$_{D4h}$**) or C_s symmetric (**TS1**) transition state for (a) AlH_4^- and (b) SiH_4. The relative electronic energy is shown as a dashed line. Stationary points are marked with red stars. The IRC calculations were done on the CCSD(T)/aug-cc-pwCVTZ(-PP) level, and the determination of molecular orbital energies was on the B97M-D3(BJ)/def2-QZVPP computational level.

TABLE IV. Molecular representations and electronic energies of the sawhorse and the pyramidal configuration. All numbers (kJ mol^{-1}) are relative to the respective tetrahedral ground states and were obtained on the CCSD(T)/aug-cc-pwCVQZ (-PP)//CCSD(T)/aug-cc-pwCVTZ(-PP) computational level.

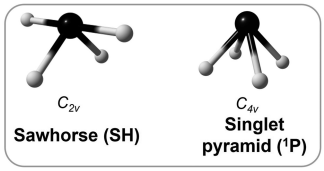

	BH_4^-	AlH_4^-	GaH_4^-	InH_4^-	TlH_4^-
SH	194.3	172.8	167.5	145.1	116.8
^{1}P	426.1	360.0	326.3	301.2	228.1

	CH_4	SiH_4	GeH_4	SnH_4	PbH_4
SH	233.0	211.2	196.2	169.2	144.2
^{1}P	468.7	351.2	303.1	277.4	188.2

	NH_4^+	PH_4^+	AsH_4^+	SbH_4^+	BiH_4^+
SH	245.9	223.1	204.8	179.0	154.7
^{1}P	439.1	318.1	267.5	246.1	154.5

undergoes oxidative (re)addition (*stepwise C_s-inversion*) depends on whether these two final reaction steps (H_2 rotation and oxidative addition) are enthalpically more favorable than the dissociation of **Int** into ^{1}[**EH_2^n**] and H_2 (**Int** ⟶ **EH_2^n** + H_2). This comparison (Table III, entry 4 vs entry 5) reveals that the *stepwise C_s-inversion* is very likely for PH_4^+ and AsH_4^+. Here, the differences between dissociation enthalpy and oxidative addition enthalpy are large and favor the reformation of the tetrahedron over the dissociation. For SiH_4, the two enthalpies are similar (18 vs 22 kJ mol^{-1}), slightly in favor of the inversion process. For the other considered hydrides, the expulsion of H_2 from **Int** is more favorable than the oxidative addition by at least 40 kJ mol^{-1}. Overall, based on the herein presented results, it can be stated that the tetrahedral hydrides of Ga, Ge, In, Sn, Sb, Tl, Pb, and Bi cannot undergo intramolecular stereochemical inversion.

Evaluation of alternative geometries

Aiming for an exhaustive understanding of the PESes of *p*-block tetrahedrons, the pyramidal and the sawhorse (SH) structural motives of the singlet electronic configuration (Table IV) were investigated (for the generally higher energy pyramidal triplet states, see the supplementary material). These structural arrangements are of practical relevance for reactivity enhancement by structural constraints (see below).[89–98]

The *pyramids* are between 469 and 155 kJ mol^{-1} higher in electronic energy than the tetrahedral ground states. In general, the energy required for pyramidalization decreases within a given group and from left to right within the Periodic Table. For the second-period elements, CH_4 has the highest energy demand (469 kJ mol^{-1}), followed by NH_4^+ (439 kJ mol^{-1}) and BH_4^- (426 kJ mol^{-1}). Compared to the D_{4h} structures, group 13 pyramids are higher in energy, whereas for groups 14 (except for methane) and 15, pyramidalization of the square planar arrangement results in an energetic lowering. This agrees with earlier results obtained for methane, silane, and germane on the Hartree–Fock and DFT computational level.[6] The harmonic frequencies of the singlet pyramids were calculated, and either two or three imaginary modes were obtained—except for the NH_4^+, which has only one imaginary vibration (cf. Table II).

The *sawhorse* (**SH**) configurations are energetically much less demanding than the pyramidal configurations and are only between 246 and 117 kJ mol^{-1} higher in electronic energy than the tetrahedral ground states. They are no stationary points on the respective PESs. The optimized non-linear *trans*-valence angles are around 100°. As found for the pyramidal configurations, the energy demand for the deformation to the **SH** structure declines from top to bottom and left to right within the *p*-block. Notably, the **SH** configurations have lower energies when compared to the lowest energy square planar states.

Evaluating the effect of structural deformation on orbital energies—A glance on synthetic application

The experimental realization of square-planar coordinated *p*-block elements is a challenging yet worthwhile task, which was

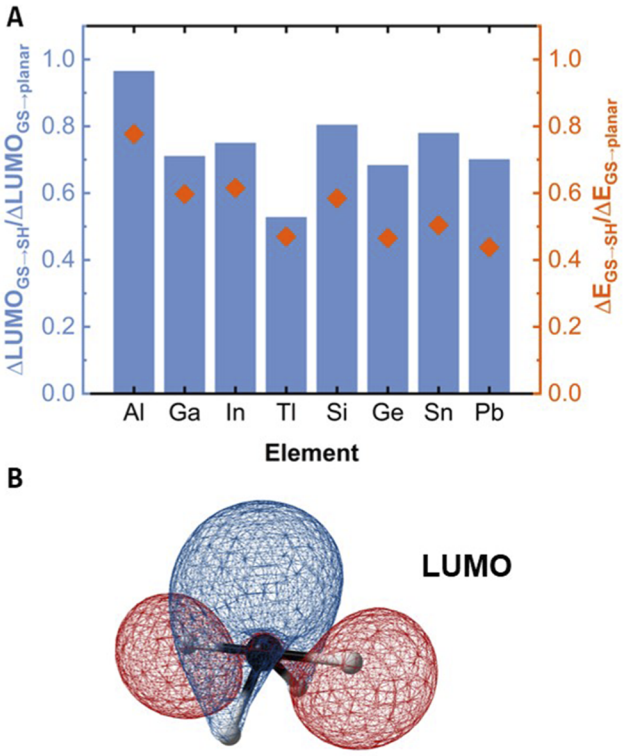

FIG. 5. (a) LUMO lowering for the **SH** configuration relative to the LUMO lowering achievable through full planarization (blue bars) and deformation energy required for the distortion to the **SH** structure relative to the planarization energy (orange squares) for **EH_4^n** (**E** = Al^-, Ga^-, In^-, Tl^-, Si, Ge, Sn, and Pb). (b) Lowest unoccupied Kohn–Sham molecular orbital (LUMO) of the **SH** structure of SiH_4. MO energies were calculated with B97M-D3(BJ)/def2-QZVPP, and deformation energies were calculated with CCSD(T)/aug-cc-pwCVQZ(-PP).

accomplished in the past for a few examples, including Al, Si, or P.[35,38,41–44] Those square planar compounds are furnished with unique reactivities that are provoked by the significant reduction of the HOMO–LUMO gap and, in particular, by lowering of the LUMO [cf. Fig. 2(a)]. To investigate whether the alternative structural deformation to the **SH** structure might enable likewise beneficial electronic effects, we examined the orbital energies of the **SH** configurations through DFT. Figure 5(a) shows the LUMO lowering when going from the tetrahedral ground states to the **SH** structures ($\Delta LUMO_{GS\longrightarrow SH}$) relative to the change that occurs when going from the ground to the square planar state ($\Delta LUMO_{GS\longrightarrow planar}$) (blue bars). The analogous relation was plotted for the electronic energy penalties [orange squares, Fig. 5(a); required energy to distort to the **SH** structure divided by the energy upon distortion to the lowest energy square planar state]. Generally, the relative deformation energy is lower than the relative LUMO lowering. For example, in the case of SiH_4, the deformation to the **SH** configuration requires 211 kJ mol^{-1}, which is 56% of the energy demand for complete planarization (379 kJ mol^{-1}), but the **SH** LUMO [shown in Fig. 5(b)] has already reached 80% of the lowering achievable through the D_{4h} symmetric structure. This effect is larger for group 14 than for group 13 compounds. These results generally predict a more straightforward experimental realization of compounds with **SH** structurally constrained *p*-block elements while maintaining large parts of the "electronic benefits" from complete planarization. Interestingly, the **SH** arrangement of carbon was already experimentally reported[99] and computationally investigated.[100]

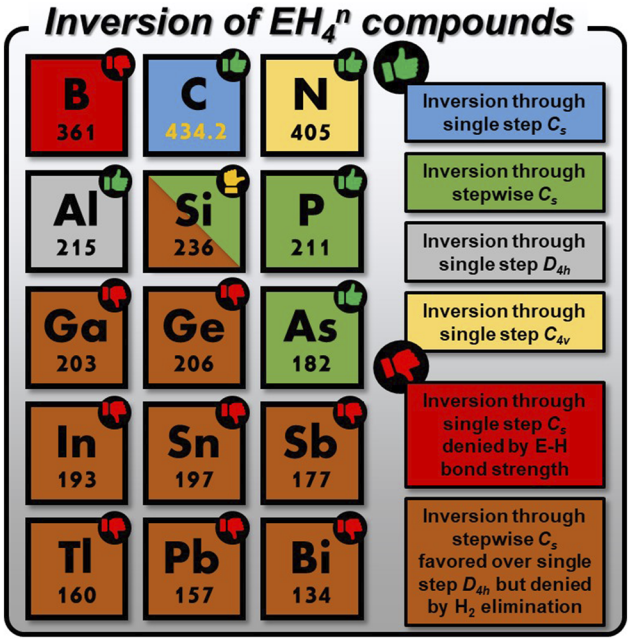

FIG. 6. Behavior of the considered *p*-block element hydrides $\mathbf{EH_4^n}$ with respect to stereochemical inversion. The numbers specify the activation enthalpy of the rate-determining step of the lowest energy inversion mechanism in kJ mol^{-1}. The calculations were done on the CCSD(T)/aug-cc-pwCVQZ(-PP)//CCSD(T)/aug-cc-pwCVTZ(-PP) level of theory, except for CH_4, for which the mHEAT+ procedure was applied.

CONCLUSION

In this paper, the element hydrides of group 13, 14, and 15 elements ($\mathbf{EH_4^n}$, $\mathbf{E^n}$ = B^-, Al^-, Ga^-, In^-, Tl^-, C, Si, Ge, Sn, Pb, N^+, P^+, As^+, Sb^+, and Bi^+) were investigated in the square planar D_{4h} and other lower-symmetrical structures. The potential energy "landscape" of inversion is curtailed by competing reactions, such as H_2 elimination or homolytic and heterolytic E–H bond rupture, respectively. Based on CCSD(T) and MRCI+Q electronic structure methods, a compilation of 206 structures and electronic configurations was evaluated with respect to the tetrahedral ground states, spanning the essential space for stereochemical inversion of tetrahedral *p*-block element compounds. The key findings are presented in the following for each element individually (Fig. 6).

- For BH_4^-, a non-planar *single-step* C_s *inversion* transition state was found. However, BH_4^- preferentially expels a hydride, prohibiting stereoinversion.
- Strikingly, the inversion of CH_4 seems not to be forbidden by CH-bond rupture—as assumed previously—but *single-step* C_s *inversion* is indeed an enthalpically feasible process with an activation enthalpy of 434.2 kJ mol^{-1}.
- NH_4^+ can undergo inversion via a unique C_{4v} symmetric transition state, which is not prevented by other pathways.
- AlH_4^- is the sole tetrahedral *p*-block element hydride that may invert via a square-planar D_{4h} symmetric transition structure (such as many other substituted *p*-block element compounds[50]).
- SiH_4, PH_4^+, and AsH_4^+ invert through a *stepwise* C_s *symmetric* process that may be regarded as a partial reductive elimination, rotation of the H_2 fragment, and oxidative addition sequence. This process is enthalpically favored over H_2 expulsion and square planar inversion.
- The unimolecular stereoinversion of GaH_4^-, InH_4^-, TlH_4^-, GeH_4, SnH_4, PbH_4, SbH_4^+, and BiH_4^+ is enthalpically not feasible. H_2 elimination is preferred instead.

Finally, pyramidal and sawhorse configurations were compared to the D_{4h} and C_s symmetric structures. The sawhorse constraint affects orbital energies in a similar fashion as complete planarization at a significantly reduced energetic expense. This finding will guide new experimental approaches for ligand design in precise frontier molecular orbital engineering.

SUPPLEMENTARY MATERIAL

See the supplementary material for full computational details, further data, and additional discussions. All calculated xyz coordinates and molecular energies are given in a separate file.

ACKNOWLEDGMENTS

Financial support was provided by the DFG (Grant No. GR5007/2-1) and the European Research Council (ERC) under the European Union's Horizon 2020 Research and Innovation Program (Grant Agreement No. 948708). L.M.S. acknowledges the "Studienstiftung des deutschen Volkes" for a scholarship. C.E. and G.G. gratefully acknowledge the Klaus Tschira Foundation for

administrative and financial support. For computational resources, we acknowledge the state of Baden-Württemberg for support through bwHPC and the German Research Foundation (DFG) through Grant No. INST 40/575-1 FUGG (JUSTUS 2 cluster), the Interdisciplinary Center for Scientific Computing (IWR) of Heidelberg University, and the Heidelberg Institute for Theoretical Studies (HITS gGmbH).

AUTHOR DECLARATIONS

Conflict of Interest

The authors have no conflicts to disclose.

DATA AVAILABILITY

The data that support the findings of this study are available within the article and its supplementary material.

REFERENCES

[1] H. J. Monkhorst, Chem. Commun. **1968**, 1111.
[2] R. Hoffmann, R. W. Alder, and C. F. Wilcox, J. Am. Chem. Soc. **92**, 4992 (1970).
[3] R. Hoffmann, Pure Appl. Chem. **28**, 181 (1971).
[4] J. B. Collins, J. D. Dill, E. D. Jemmis, Y. Apeloig, P. von Ragué Schleyer, R. Seeger, and J. A. Pople, J. Am. Chem. Soc. **98**, 5419 (1976).
[5] K. Yoshizawa, A. Suzuki, and T. Yamabe, J. Am. Chem. Soc. **121**, 5266 (1999).
[6] K. Yoshizawa and A. Suzuki, Chem. Phys. **271**, 41 (2001).
[7] K. Yoshizawa, J. Organomet. Chem. **635**, 100 (2001).
[8] R. Keese, Chem. Rev. **106**, 4787 (2006).
[9] L.-M. Yang, E. Ganz, Z. Chen, Z.-X. Wang, and P. von Ragué Schleyer, Angew. Chem., Int. Ed. **54**, 9468 (2015).
[10] M. S. Gordon and M. W. Schmidt, J. Am. Chem. Soc. **115**, 7486 (1993).
[11] M. J. M. Pepper, I. Shavitt, P. von Ragué Schleyer, M. N. Glukhovtsev, R. Janoschek, and M. Quack, J. Comput. Chem. **16**, 207 (1995).
[12] O. Dobis and S. W. Benson, Int. J. Chem. Kinet. **19**, 691 (1987).
[13] Y.-R. Luo, *Comprehensive Handbook of Chemical Bond Energies* (CRC Press, Hoboken, 2007).
[14] D. J. Grant, A. J. Arduengo, and D. A. Dixon, J. Phys. Chem. A **113**, 750 (2009).
[15] E.-U. Würthwein and P. von Ragué Schleyer, Angew. Chem., Int. Ed. **18**, 553 (1979).
[16] D. A. Dixon and A. J. Arduengo, J. Phys. Chem. **91**, 3195 (1987).
[17] D. A. Dixon and A. J. Arduengo III, Int. J. Quantum Chem. **34**, 85 (1988).
[18] A. I. Boldyrev, P. von Ragué Schleyer, and R. Keese, Mendeleev Commun. **2**, 93 (1992).
[19] M. P. McGrath and L. Radom, J. Am. Chem. Soc. **115**, 3320 (1993).
[20] D. R. Rasmussen and L. Radom, Angew. Chem., Int. Ed. **38**, 2875 (1999).
[21] S.-D. Li, G.-M. Ren, C.-Q. Miao, and Z.-H. Jin, Angew. Chem., Int. Ed. **43**, 1371 (2004).
[22] U. D. Priyakumar, A. S. Reddy, and G. N. Sastry, Tetrahedron Lett. **45**, 2495 (2004).
[23] G. Merino, M. A. Méndez-Rojas, A. Vela, and T. Heine, J. Comput. Chem. **28**, 362 (2007).
[24] H.-b. Xie and Y.-h. Ding, J. Chem. Phys. **126**, 184302 (2007).
[25] C. Zhang, W. Sun, and Z. Cao, J. Am. Chem. Soc. **130**, 5638 (2008).
[26] Y. Li, F. Li, Z. Zhou, and Z. Chen, J. Am. Chem. Soc. **133**, 900 (2011).
[27] Z.-h. Cui, M. Contreras, Y.-h. Ding, and G. Merino, J. Am. Chem. Soc. **133**, 13228 (2011).
[28] A. C. Castro, M. Audiffred, J. M. Mercero, J. M. Ugalde, M. A. Méndez-Rojas, and G. Merino, Chem. Phys. Lett. **519-520**, 29 (2012).
[29] O. Yañez, A. Vásquez-Espinal, R. Pino-Rios, F. Ferraro, S. Pan, E. Osorio, G. Merino, and W. Tiznado, Chem. Commun. **53**, 12112 (2017).
[30] M.-J. Sun, X. Cao, and Z. Cao, Nanoscale **10**, 10450 (2018).
[31] V. Vassilev-Galindo, S. Pan, K. J. Donald, and G. Merino, Nat. Rev. Chem. **2**, 0114 (2018).
[32] Y. Zhang, C. Zhang, Y. Mo, and Z. Cao, Chem. - Eur. J. **27**, 1402 (2021).
[33] M.-h. Wang, M. Orozco-Ic, L. Leyva-Parra, W. Tiznado, J. Barroso, Y.-h. Ding, Z.-h. Cui, and G. Merino, J. Phys. Chem. A **125**, 3009 (2021).
[34] N. Job, M. Khatun, K. Thirumoorthy, S. S. Reddy CH, V. Chandrasekaran, A. Anoop, and V. S. Thimmakondu, Atoms **9**, 24 (2021).
[35] M. Driess, J. Aust, K. Merz, and C. van Wüllen, Angew. Chem., Int. Ed. **38**, 3677 (1999).
[36] X. Li, L.-S. Wang, A. I. Boldyrev, and J. Simons, J. Am. Chem. Soc. **121**, 6033 (1999).
[37] X. Li, H.-F. Zhang, L.-S. Wang, G. D. Geske, and A. I. Boldyrev, Angew. Chem., Int. Ed. **39**, 3630 (2000).
[38] D. W. Stephan, Angew. Chem., Int. Ed. **39**, 501 (2000).
[39] E. J. Thompson, T. W. Myers, and L. A. Berben, Angew. Chem., Int. Ed. **53**, 14132 (2014).
[40] J. Xu, X. Zhang, S. Yu, Y.-h. Ding, and K. H. Bowen, J. Phys. Chem. Lett. **8**, 2263 (2017).
[41] F. Ebner and L. Greb, J. Am. Chem. Soc. **140**, 17409 (2018).
[42] F. Ebner, H. Wadepohl, and L. Greb, J. Am. Chem. Soc. **141**, 18009 (2019).
[43] F. Ebner, P. Mainik, and L. Greb, Chem. - Eur. J. **27**, 5120 (2021).
[44] F. Ebner and L. Greb, Chem **7**, 2151 (2021).
[45] T. M. Bass, C. R. Carr, T. J. Sherbow, J. C. Fettinger, and L. A. Berben, Inorg. Chem. **59**, 13517 (2020).
[46] M. B. Krogh-Jespersen, J. Chandrasekhar, E. U. Wuerthwein, J. B. Collins, and P. von Ragué Schleyer, J. Am. Chem. Soc. **102**, 2263 (1980).
[47] D. A. Dixon and A. J. Arduengo III, J. Chem. Soc., Chem. Commun. **1987**, 498.
[48] S. Raghunathan, K. Yadav, V. C. Rojisha, T. Jaganade, V. Prathyusha, S. Bikkina, U. Lourderaj, and U. D. Priyakumar, Phys. Chem. Chem. Phys. **22**, 14983 (2020).
[49] K. Yadav, U. Lourderaj, and U. D. Priyakumar, Atoms **9**, 79 (2021).
[50] L. M. Sigmund, R. Maier, and L. Greb, Chem. Sci. **13**, 510 (2022).
[51] H. A. Jahn and E. Teller, Proc. R. Soc. London, Ser. A **161**, 220 (1937).
[52] I. B. Bersuker, N. N. Gorinchoi, and V. Z. Polinger, J. Mol. Struct. **270**, 369 (1992).
[53] I. B. Bersuker, Chem. Rev. **113**, 1351 (2013).
[54] I. B. Bersuker, Chem. Rev. **121**, 1463 (2021).
[55] T. A. Albright, J. K. Burdett, and M.-H. Whangbo, *Orbital Interactions in Chemistry* (Wiley, Hoboken, NJ, 2013).
[56] B. O. Roos, P. R. Taylor, and P. E. M. Sigbahn, Chem. Phys. **48**, 157 (1980).
[57] H. J. Werner and P. J. Knowles, J. Chem. Phys. **89**, 5803 (1988).
[58] P. J. Knowles and H.-J. Werner, Chem. Phys. Lett. **145**, 514 (1988).
[59] H.-J. Werner, P. J. Knowles, G. Knizia, F. R. Manby, and M. Schütz, Wiley Interdiscip. Rev.: Comput. Mol. Sci. **2**, 242 (2012).
[60] H.-J. Werner, P. J. Knowles, F. R. Manby, J. A. Black, K. Doll, A. Heßelmann, D. Kats, A. Köhn, T. Korona, D. A. Kreplin, Q. Ma, T. F. Miller III, A. Mitrushchenkov, K. A. Peterson, I. Polyak, G. Rauhut, and M. Sibaev, J. Chem. Phys. **152**, 144107 (2020).
[61] G. D. Purvis III and R. J. Bartlett, J. Chem. Phys. **76**, 1910 (1982).
[62] K. Raghavachari, G. W. Trucks, J. A. Pople, and M. Head-Gordon, Chem. Phys. Lett. **157**, 479 (1989).
[63] J. D. Watts, J. Gauss, and R. J. Bartlett, J. Chem. Phys. **98**, 8718 (1993).
[64] F. Neese, Wiley Interdiscip. Rev.: Comput. Mol. Sci. **2**, 73 (2012).
[65] F. Neese, Wiley Interdiscip. Rev.: Comput. Mol. Sci. **8**, e1327 (2018).
[66] D. J. Goebbert and P. G. Wenthold, Int. J. Mass Spectrom. **257**, 1 (2006).
[67] D. B. Workman and R. R. Squires, Inorg. Chem. **27**, 1846 (1988).
[68] A. Tajti, P. G. Szalay, A. G. Császár, M. Kállay, J. Gauss, E. F. Valeev, B. A. Flowers, J. Vázquez, and J. F. Stanton, J. Chem. Phys. **121**, 11599 (2004).
[69] Y. J. Bomble, J. Vázquez, M. Kállay, C. Michauk, P. G. Szalay, A. G. Császár, J. Gauss, and J. F. Stanton, J. Chem. Phys. **125**, 064108 (2006).

[70]M. E. Harding, J. Vázquez, B. Ruscic, A. K. Wilson, J. Gauss, and J. F. Stanton, J. Chem. Phys. **128**, 114111 (2008).
[71]J. H. Thorpe, C. A. Lopez, T. L. Nguyen, J. H. Baraban, D. H. Bross, B. Ruscic, and J. F. Stanton, J. Chem. Phys. **150**, 224102 (2019).
[72]D. A. Matthews, L. Cheng, M. E. Harding, F. Lipparini, S. Stopkowicz, T.-C. Jagau, P. G. Szalay, J. Gauss, and J. F. Stanton, J. Chem. Phys. **152**, 214108 (2020).
[73]Minimum structure optimizations confirmed them as local minima on the respective potential energy surfaces. For InH_4^- and TlH_4^-, the frequency analyses gave in each case a small imaginary frequency (87i and 144i cm^{-1}). Hence, the obtained **Int** structures cannot be considered as true local minimum structures. As it is shown, this is not of significant relevance.
[74]R. S. Grev and H. F. Schaefer, J. Chem. Soc., Chem. Commun. **1983**, 785.
[75]M. S. Gordon, D. R. Gano, J. S. Binkley, and M. J. Frisch, J. Am. Chem. Soc. **108**, 2191 (1986).
[76]C. Sosa and H. B. Schlegel, J. Am. Chem. Soc. **106**, 5847 (1984).
[77]I. S. Ignatyev and H. F. Schaefer, J. Am. Chem. Soc. **119**, 12306 (1997).
[78]R. Becerra, S. E. Boganov, M. P. Egorov, V. I. Faustov, O. M. Nefedov, and R. Walsh, Can. J. Chem. **78**, 1428 (2000).
[79]G. Merino, S. Escalante, and A. Vela, J. Phys. Chem. A **108**, 4909 (2004).
[80]Y. Wang and J. Ma, J. Organomet. Chem. **694**, 2567 (2009).
[81]S. E. Boganov, V. M. Promyslov, V. I. Faustov, M. P. Egorov, and O. M. Nefedov, Russ. Chem. Bull. **60**, 2147 (2011).
[82]X. Wang, L. Andrews, G. V. Chertihin, and P. F. Souter, J. Phys. Chem. A **106**, 6302 (2002).
[83]X. Wang, L. Andrews, and G. P. Kushto, J. Phys. Chem. A **106**, 5809 (2002).
[84]L. Andrews and X. Wang, J. Phys. Chem. A **106**, 7696 (2002).
[85]X. Wang and L. Andrews, J. Am. Chem. Soc. **125**, 6581 (2003).
[86]R. P. Bell, Proc. R. Soc. London, Ser. A **154**, 414 (1936).
[87]M. G. Evans and M. Polanyi, Trans. Faraday Soc. **34**, 11 (1938).
[88]P. Muller, Pure Appl. Chem. **66**, 1077 (1994).
[89]W. Zhao, S. M. McCarthy, T. Y. Lai, H. P. Yennawar, and A. T. Radosevich, J. Am. Chem. Soc. **136**, 17634 (2014).
[90]T. P. Robinson, D. M. De Rosa, S. Aldridge, and J. M. Goicoechea, Angew. Chem., Int. Ed. Engl. **54**, 13758 (2015).
[91]Y.-C. Lin, E. Hatzakis, S. M. McCarthy, K. D. Reichl, T.-Y. Lai, H. P. Yennawar, and A. T. Radosevich, J. Am. Chem. Soc. **139**, 6008 (2017).
[92]S. Volodarsky and R. Dobrovetsky, Chem. Commun. **54**, 6931 (2018).
[93]J. C. Gilhula and A. T. Radosevich, Chem. Sci. **10**, 7177 (2019).
[94]A. Brand and W. Uhl, Chem. - Eur. J. **25**, 1391 (2019).
[95]G. T. Cleveland and A. T. Radosevich, Angew. Chem., Int. Ed. **58**, 15005 (2019).
[96]L. M. Sigmund and L. Greb, Chem. Sci. **11**, 9611 (2020).
[97]F. Ebner, L. M. Sigmund, and L. Greb, Angew. Chem., Int. Ed. **59**, 17118 (2020).
[98]L. M. Sigmund, C. Ehlert, M. Enders, J. Graf, G. Gryn'ova, and L. Greb, Angew. Chem., Int. Ed. **60**, 15632 (2021).
[99]R. E. von H. Spence, D. J. Parks, W. E. Piers, M.-A. MacDonald, M. J. Zaworotko, and S. J. Rettig, Angew. Chem., Int. Ed. **34**, 1230 (1995).
[100]U. Radius, S. J. Silverio, R. Hoffmann, and R. Gleiter, Organometallics **15**, 3737 (1996).